Angular and spectral sensitivity of fly photoreceptors. III. Dependence on the pupil mechanism in the blowfly Calliphora

Stavenga, Doekele

Published in:
Journal of comparative physiology a-Neuroethology sensory neural and behavioral physiology

DOI:
10.1007/s00359-003-0477-0

Publication date:
2004

J Comp Physiol A (2004) 190: 115–129
DOI 10.1007/s00359-003-0477-0

ORIGINAL PAPER

D. G. Stavenga

Angular and spectral sensitivity of fly photoreceptors. III. Dependence on the pupil mechanism in the blowfly *Calliphora*

Received: 2 June 2003 / Revised: 5 November 2003/Accepted: 7 November 2003 / Published online: 9 January 2004

Abstract A wave optics model for the facet lens-rhabdomere system of fly eyes is used to analyze the dependence of the angular and spectral sensitivity of R1–6 photoreceptors on the pupil mechanism. This assembly of light-absorbing pigment granules in the soma interacts with the waveguide modes propagating in the rhabdomere. A fly rhabdomere carries two modes in the middle wavelength range and four modes at short wavelengths, depending on the rhabdomere diameter and the angle of the incident light flux. The extension of the mode to outside the rhabdomere strongly depends on wavelength, and this dependence plays a determinant role in the light control function of the pupil. The absorbance spectrum of the pigment in the pupil granules is severely depressed at short wavelengths by waveguide effects, resulting in a distinct blue peak. Accordingly, pupil closure suppresses the photoreceptor's spectral sensitivity much more in the blue-green than in the UV. The pupil only narrows the angular sensitivity at short wavelengths. The geometrical size of the rhabdomere governs the angular sensitivity of fly photoreceptors in the dark-adapted state, but diffraction takes over in the fully light-adapted state.

Keywords Boundary wave · Diffraction limit · Light-adaptation · Optical waveguides · Sensitizing pigment · Spectral shift

Introduction

Photoreceptors sample optical information from the environment via light absorption by the visual pigments that are concentrated in specialized organelles, the rods and cones of vertebrates and the rhabdomeres and rhabdoms of insects and crustaceans. In the eyes of flies, the facet lenses and the photoreceptors' rhabdomeres form an array of integrated optical systems, which determines the eyes' visual resolution. Several studies devoted to unravelling the fly retina have shown that the facet lens-rhabdomere system has reached a high degree of sophistication. The rhabdomere tips are positioned in the focal plane of the facet lens, where the light flux is most intense, the light is trapped in the rhabdomeres in optical waveguide modes, so as to realize high light capture rates by the visual pigment molecules, the rhabdomeres are tightly packed together, but they are sufficiently spatially separate to avoid optical coupling, and the cross-sections of the rhabdomeres are large enough to avoid substantial leakage of light (revs Kirschfeld 1974; Snyder 1979; Land 1989).

The two principal measures of a photoreceptor's performance are its angular and spectral sensitivity. The angular sensitivity function, which is usually a Gaussian-like, symmetric function, is experimentally determined with a point source of fixed wavelength whose spatial direction is varied. The light sensitivity is then normalized to the value at the photoreceptor's visual axis. The spectral sensitivity function is measured by varying the wavelength of the light emitted by a spatially fixed light source, again with subsequent normalization of the light sensitivity at the peak wavelength, λ_{max}. Experimental, theoretical and computational studies point out, however, that both angular and spectral sensitivity functions cannot be fully separated, because the angular sensitivity depends on wavelength and the spectral sensitivity depends on the spatial direction of the light source (Pask and Barrell 1980a, 1980b; van Hateren 1989).

The angular and spectral sensitivities of fly photoreceptors and their interdependence have been investigated in detail by optical modelling of a number of idealized cases, which were inspired by anatomical, optical and/or physiological data obtained from houseflies and blowflies (Stavenga 2003a) and fruitfly (Stavenga 2003b). The three optical components considered in these papers were the light-diffracting facet lens, the

D. G. Stavenga
Department of Neurobiophysics,
University of Groningen, 9747 AG Groningen, The Netherlands
E-mail: stavenga@phys.rug.nl

light-guiding rhabdomere and the light-absorbing visual pigment. Here I extend that approach by incorporating the light-controlling pupil mechanism. This system consists of screening pigment granules inside the photoreceptor soma, which absorb and scatter light when they are sufficiently near the rhabdomere boundary. Light propagating along the rhabdomere spreads to outside the rhabdomere surroundings, and the pigment granules can therefore control the light flux by varying their position in the rhabdomere vicinity (Franceschini and Kirschfeld 1976; Stavenga 1979). Pupil mechanisms exist in all fly photoreceptors, but the theme of this paper is the most prominently active system, that of the large, peripheral photoreceptors R1–6 (Franceschini 1975).

Closing the pupil has several consequences (Stavenga 1989): (1) it narrows the photoreceptor's angular sensitivity function, due to selective absorption of light from waveguide modes in the rhabdomere (Smakman et al. 1984; van Hateren 1989); (2) it blue shifts the spectral sensitivity function, also due to waveguide effects (Hardie 1979; Vogt et al. 1982); and (3) it favours photoregeneration of visual pigment, because the pupillary granules have little absorption in the long wavelength range, where the rhodopsin's photoproduct, metarhodopsin, absorbs most strongly (Stavenga et al. 1973). Previous studies provided partial explanations of the various optical consequences of the pupil. The aim of the present study is to present a more comprehensive, quantitative analysis of the pupillary effects.

Results

Anatomy of fly photoreceptors, rhabdomere waveguide optics and the pupil mechanism

The following analysis of the pupil mechanism is based on detailed published descriptions of the structure and optics of the basic optical unit of the fly compound eye, the ommatidium. A fly ommatidium is a long, cylindrical structure, capped by a facet lens, which contains six large, peripheral photoreceptors, R1–6, that span most of the length of the ommatidium and two slender, central photoreceptors, R7, 8, that together stretch the length of the ommatidium. In the housefly, *Musca*, the diameter of R1–6 rhabdomeres is distally 2.0 μm, which reduces to 1.0 μm proximally over a length of ca 200 μm (Boschek 1971). The rhabdomeres are arranged in a characteristic trapezoidal pattern. Presumably because the R1, 3, 5 and 6 rhabdomeres form the corner points, they have a somewhat larger diameter compared to that of the slightly compressed R2 and 4 (Boschek 1971; van Hateren 1984). The diameters of R1–6 rhabdomeres in the fruitfly *Drosophila* are rather similar to those of *Musca* (Masai et al. 1996), but other species have distinctly wider as well as narrower rhabdomeres, e.g., diameter $D_r > 4.0$ μm in the male blowfly *Chrysomia* (van Hateren et al. 1989), and $D_r \approx 1.3$ μm in the blowfly *Calliphora* (Wunderer and Smola 1982; review Hardie 1985). Angular sensitivities of blowfly photoreceptors, measured by electrophysiological methods and interpreted with model calculations, yielded $D_r = 1.5$–1.8 μm (Smakman et al. 1984), and related optical measurements yielded 1.8 μm (van Hateren 1984).

Small pigment granules, diameter 0.15 μm, found throughout the soma of fly photoreceptors (Trujillo-Cenoz 1972; Boschek 1971), migrate towards the rhabdomere upon illumination with bright light and move away from the rhabdomere during subsequent darkness. The diameter of the cell soma in *Drosophila*, only 3–4 μm (Masai et al. 1996), is much smaller than the 5–15 μm attained in *Musca* (Boschek 1971; Hardie 1985) and *Calliphora* (Wunderer and Smola 1982), or the 30 μm in male *Chrysomia* (van Hateren et al. 1989). The distance that the granules travel from the dark-adapted to the light-adapted state until they reach the rhabdomere vicinity thus is strongly species dependent.

Incident light, which enters a facet lens and then is focused on a rhabdomere's distal tip, excites specific spatial intensity distributions, the modes. The number of excited modes depends on the waveguide number, $V = (\pi D_r/\lambda)\sqrt{n_1^2 - n_2^2}$, where λ is the light wavelength, and n_1 and n_2 are the refractive indices of rhabdomere interior and exterior, respectively (Eq. A3). The diameter and wavelength are the two important parameters here, because the refractive indices, taken to be $n_1 = 1.363$ and $n_2 = 1.340$, are virtually constant (see Stavenga 2003a, 2003b). For *Musca* R1–6 rhabdomeres, carrying monochromatic light of wavelength $\lambda = 500$ nm, and tapering from 2.0 to 1.0 μm, the V-number drops from 3.13 at the distal tip to 1.57 at the proximal end. Because the cut-off value for the second mode is $V_{co} = 2.405$, two modes are then allowed distally, and proximally only one, the lowest order mode, exists (for details, see e.g. Stavenga 2003a). The mode shape strongly depends on the polarization, but in this paper only unpolarized light is considered. The light distribution in the modes then is circular symmetric (Appendix 1). The light fraction propagating outside the rhabdomere boundary is called the boundary wave.

When the pupillary pigment granules are sufficiently near the rhabdomere, they absorb part of the boundary wave. This reduces the light absorption by the visual pigment and consequently the photoreceptor sensitivity. A quantitative analysis of the action of the fly pupil on the photoreceptor's angular and spectral sensitivity therefore has to delineate the complex system of light excitation and propagation in the waveguide modes, as well as the spectral absorption by pupillary and visual pigments.

Road map of the analysis of photoreceptor angular and spectral sensitivity

The analysis proceeds in seven steps. The formal basis is given in the Appendices.

1. I calculate first the light distribution in the allowed waveguide modes, showing that modes spread to outside the rhabdomere boundary with increasing wavelength.
2. Then I calculate the excited light power, which is the light power channeled by the facet lens into the rhabdomere. The power available for the visual pigment is the fraction of the excited light propagating inside the rhabdomere boundary and therefore is called the effective light power. I treat two cases of rhabdomeres, i.e., when the rhabdomere has a constant diameter and when it tapers, and two different illumination conditions, i.e., an axial point source and an extended, uniform light source. It appears that the total light flux channeled into the rhabdomere is rather independent of wavelength in the dark-adapted photoreceptor, i.e., when the pupil is negligible.
3. To get a clear view on the spatial extent of the waveguide modes outside the rhabdomere and the interaction of modes and pupil, I present data of exponential fits to the boundary wave. The space constants of these exponential functions depend strongly on wavelength, especially for the higher order modes.
4. I subsequently analyze how the pupil absorbance spectrum depends on the position of the pupillary granules. It emerges that waveguide effects strongly depress the absorbance spectrum of the granules' pigment in the short-wavelength range, because the light fraction propagating outside the rhabdomere decreases with decreasing wavelength.
5. I then calculate the light absorbed by the visual pigment in the presence of a variable pupil, assuming that the pupil acts at the very distal end of the rhabdomere. The results show that the closing pupil predominantly suppresses the spectral sensitivity in the blue-green, and less in the UV, for both axial and uniform light sources.
6. In the next step I present model calculations for the angular sensitivity and compare them with experimental data of Smakman et al. (1984).
7. I finally calculate the photoreceptor acceptance angle as a function of wavelength for various pupil states, and relate the resulting data to geometrical and diffraction optics.

Waveguide modes in a fly rhabdomere

Smakman et al. (1984) reported a specific blowfly photoreceptor where the angular sensitivity was measured at a number of wavelengths in both the dark- and light-adapted state. The angular sensitivity narrowed upon light adaptation, which could be well explained by the selective absorption of the higher order modes by the pupil mechanism. A computational analysis yielded a rhabdomere diameter D_r = 1.6 μm, and for the overlying facet lens a diameter D_l = 31 μm and F-number F = 2.5. These values were chosen for most of the calculations in the present paper. Figure 1a, b presents a 1.6 μm rhabdomere and the shape of the first two modes at wavelength 400 nm, or, at V = 3.13. The diagrams of Fig. 1c and d show the profile of the modes, together with the rhabdomere and the attached soma, with the pigment granules in the dark-adapted (DA) and light-adapted (LA) state, respectively.

The number of allowed modes and their shape depend on both the rhabdomere diameter and the light wavelength. As an example, Fig. 2 considers the case where unpolarized light of various wavelengths propagates in a rhabdomere with diameter D_r = 1.6 μm. At each wavelength and for each mode the total light flux is taken to be 1 W and the resulting intensity distribution of the mode is shown. The choice of 1 W for the unit of incident light flux may seem to be in conflict with the basic knowledge that photoreceptors deal with photons, but with 1 photon per second for the incident light flux at the facet lens the intensity in the rhabdomere would be a fraction of a photon per second per μm^2, which is odd and clumsy. Anyhow, the dimension of the intensity, W μm^{-2}, vanishes from calculations of angular and spectral sensitivities due to normalization, and when the incident photon flux is known, it is a simple step to recalculate the local intensities in photon numbers.

Excited and effective light power with an axial point source and a uniform light source in the dark-adapted state

The sensitivity spectrum of a fly photoreceptor is primarily determined by the absorption spectrum of its

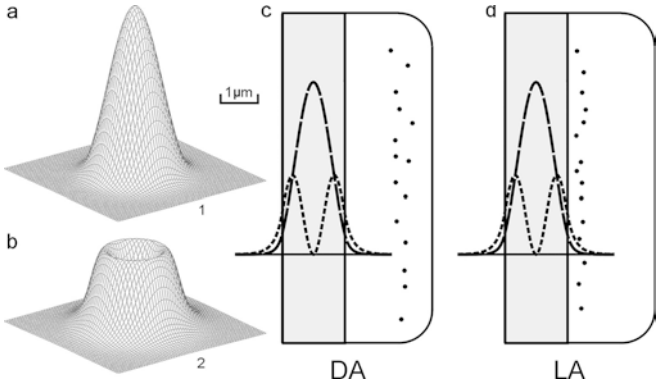

Fig. 1a–d Diagrams of modes and pupil mechanism in a photoreceptor cell with a circular cylindrical rhabdomere, diameter D_r = 1.6 μm. **a** Spatial light intensity distribution of the first mode (p = 1) at wavelength λ = 400 nm. **b** Second mode (p = 2) at 400 nm. **c** Profiles of the two modes showing that the second mode extends to further outside the rhabdomere then the first mode. The modes propagate unhindered in the dark-dapted (*DA*), state when the pigment granules in the soma are remote from the rhabdomere. d Upon light-adaption (*LA*) pigment granules migrate towards the rhabdomere boundary. When the granules approach the rhabdomere, they first attenuate the boundary wave of the second mode. Under extreme adaptation, when the granules are very near the rhabdomere, they also absorb light propagating in the boundary wave of the first mode

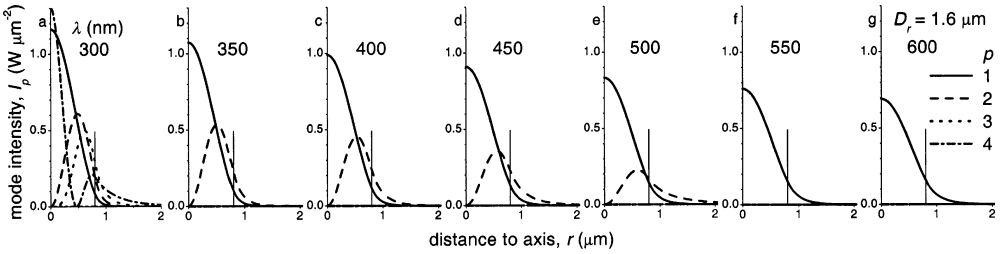

Fig. 2 Intensity profiles of the modes, p =1–4, propagating in a 1.6 μm rhabdomere at different wavelengths, λ. The rhabdomere border (at $r = b = 0.8$ μm) is indicated by a thin vertical line. For 550 and 600 nm light only the first mode ($p = 1$) is allowed. At 350, 400, 450 and 500 nm two modes ($p = 1, 2$) can exist, and at 300 nm the first four modes (p =1–4) propagate. The modes extend increasingly to outside the rhabdomere with increasing wavelength λ and mode number p. This decreases the peak intensity with increasing wavelength for each mode, since the total light power propagating in the rhabdomere at all wavelengths is 1 W

visual pigment, but the amount of incident light that is channeled into the rhabdomere is not equal for all wavelengths, due to the wavelength dependence of both the facet lens' diffraction optics and the rhabdomere's waveguide optics (Stavenga 2003b; Appendix 3). Figure 3 (upper curve) gives the excited power, P_{exc}, as a function of wavelength for an axial point source illuminating an $F = 2.5$ facet lens with in its focal plane the tip of a 1.6 μm rhabdomere. Axial light excites virtually exclusively the first mode, except for wavelengths below 326 nm, the cut-off wavelength of mode $p = 4$ (Stavenga 2003a). The total excited power channelled into the rhabdomere, obtained by summing the excited mode powers, is virtually independent of wavelength: $P_{exc} \approx 0.8$ W; i.e., about 80% of axial light enters the rhabdomere.

In the fully dark-adapted state pupil absorption is absent, and then a fraction $\left\{1 - \exp\left\lfloor -\bar{\eta}_p(\lambda)\kappa_v(\lambda)L\right\rfloor\right\}$ of the light power excited in mode p is absorbed by the visual pigment; here $\bar{\eta}_p$ is the averaged light power fraction of mode p propagating inside the rhabdomere (see Eq. A6a), κ_v is the absorption coefficient of the rhabdomere medium, and L is the rhabdomere length (see Eq. A17 and Stavenga 2003b). When $\kappa_v L$ is small, a simple expression for the absorbed light power follows (Eq. A18): $P_{abs}(\lambda) = \kappa_v(\lambda)LP_{eff}(\lambda)$. With axial illumination $P_{eff}(\lambda) = P_{1,eff}(\lambda) + P_{4,eff}(\lambda) = P_{1,exc}\bar{\eta}_1(\lambda) + P_{4,exc}\bar{\eta}_4(\lambda)$. Figure 3 presents $P_{eff}(\lambda)$ for a rhabdomere with a constant diameter of 1.6 μm (non-taper) and a rhabdomere tapering parabolically from a distal diameter 1.6 μm to a proximal value 1.0 μm (taper; see Boschek 1971, and Stavenga 2003b). The light power fractions $\bar{\eta}_1(\lambda)$ and $\bar{\eta}_4(\lambda)$ decrease the absorption efficiency of the visual pigment with increasing wavelength, and the decrease is somewhat stronger in the tapering rhabdomere. The precise shape of the tapering, whether parabolic or linear, appears to have only minor effects on the final effective light power spectrum.

Fly photoreceptors normally receive light from extended light sources. Integration of the excited light power function over the angle then yields the excited light power (Stavenga 2003b). Assuming for the irradiance of a uniform, monochromatic light source 1 W sr^{-1} μm^{-2}, and considering again first a dark-adapted or pupil-less photoreceptor, the excited power spectrum in the 1.6 μm rhabdomere is given in Fig. 4a. The excitation of the modes appears to depend strongly on wavelength (Fig. 4a). The effective power of mode p is again obtained by multiplying the light power excited in mode p with the effective light power fraction, $\bar{\eta}_p$. With respect to the total excited power spectrum (Fig. 4a, bold line), the total effective power spectrum, i.e., the sum of the effective mode power spectra, is considerably flattened in the non-tapering rhabdomere (Fig. 4b), and even more so in the tapering rhabdomere (Fig. 4c).

The rhabdomere boundary wave

Figure 2 shows that some of the light propagates outside the rhabdomere. The outside fraction, the so-called boundary wave, increases with the mode number, and for a given mode with wavelength. The radial light intensity distribution of a mode outside the rhabdomere well approximates an exponential function (Appendix 1, Eq. A7), $\bar{I}_p(r) = B_p\exp[-(r-b)/\rho_p]$, where B_p is the intensity of mode p at the rhabdomere border (Fig. 5a), r is the radial distance to the rhabdomere axis, $b = D_r/2$ is the rhabdomere radius, and ρ_p is the space constant of the boundary wave (Fig. 5b). As explained in Appendix 2, using data of exponential fits considerably simplifies the calculation procedures, and more importantly, it facilitates the understanding of how the pupil affects the boundary waves. For instance, Fig. 5b shows that the space constant for all modes p is extremely small, $\rho_p \leq 0.3$ μm, except near the cut-off wavelengths, where the boundary waves spread more.

The quality of the exponential fits can be assessed by calculating for each mode the fraction of the light power propagating outside the rhabdomere, ζ_p, as predicted by waveguide theory (Eq. A6b; bold curves in Fig. 5c) and by the exponential fit: $\zeta_p = 2\pi B_p\rho_p(\rho_p + b)$ (Eq. A8; thin curves in Fig. 5c). The bold and thin curves for the first mode ($p = 1$) coincide, but the two curves start to deviate near the cut-off wavelengths of the higher order modes; there the exponential function underestimates the propagated light power of the boundary wave (Fig. 5c). The bold curves in Fig. 5b correct for this error (Eq. A9, and see Appendix 1 for further explanation).

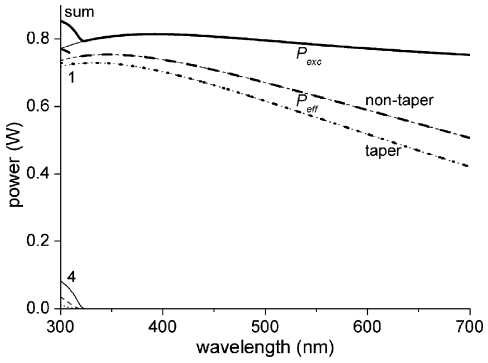

Fig. 3 Light power as a function of wavelength in a fly rhabdomere illuminated by an axial point source. The distal end of the rhabdomere, diameter D_r = 1.6 μm, coincides with the focal plane of a facet lens with F-number F = 2.5, and a total power of 1 W passes the facet lens at all wavelengths. P_{exc} is the light power excited in the rhabdomere, and P_{eff} is the light power available for absorption by the visual pigment. Virtually all excited light power is carried by mode 1, and mode 4 is only excited appreciably near 300 nm. The light power excited in mode 1 is $P_{1,exc} \approx 0.8$ W throughout the total wavelength range. The effective light power in mode 1, $P_{1,eff} = P_{1,exc}\bar{\eta}_1$ is the excited light power times the averaged light power fraction propagated inside the rhabdomere, $\bar{\eta}_1$. The latter factor is calculated for a rhabdomere with a constant diameter of D_r = 1.6 μm (non-taper) as well as for a rhabdomere tapering from 1.6 μm to 1.0 μm (taper), according to $D_r = [1.6–0.6(z/L)^2]$; z is the longitudinal coordinate of the rhabdomere with length L. The tapering slightly decreases the effective light power and this effect increases with wavelength. The curves for the powers of the individual modes (p = 1 and p = 4) are thin, and the curves for their sums are bold

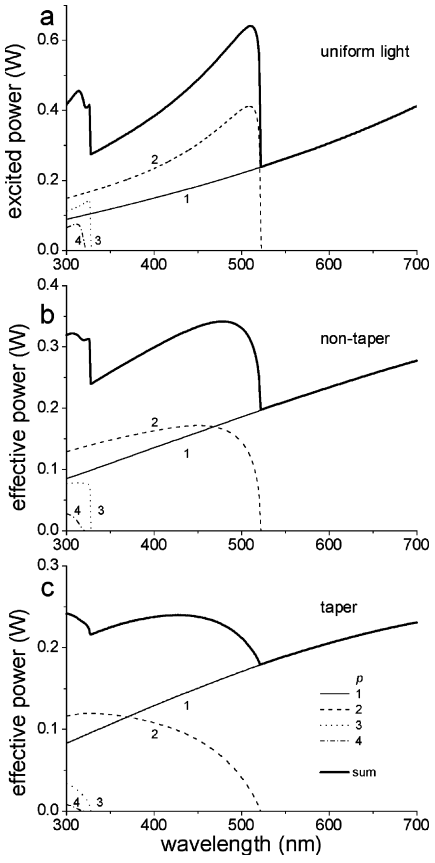

Fig. 4a–c Excited and effective light power in a fly rhabdomere when illuminated by a monochromatic, uniform light source. The same facet lens-rhabdomere combination as that of Fig. 3 receives an irradiance of 1 W sr^{-1} μm^{-2} at all wavelengths. **a** Excited power of modes 1–4 and their sum. **b** Effective power of modes 1–4 and their sum for a rhabdomere with a constant diameter of D_r = 1.6 μm. **c** Excited power of modes 1–4 and their sum for a rhabdomere tapering from 1.6 μm to 1.0 μm. The relative contribution of the higher modes decreases due to the stronger filtering by the waveguide, specifically of mode 2 in the tapering rhabdomere

The pupil can be visualized as an assembly of pigment granules, uniformly distributed in the soma up to a border that is a distance h from the rhabdomere, referred to as the pupil distance (Fig. 6, inset). The fraction of the light power propagating in mode p outside the cylinder with radius $s = b + h$, given by (Eq. A15), $\epsilon_p(s) = 2\pi B_p \rho_p(\rho_p + s)\exp(-h/\rho_p)$ changes characteristically with wavelength (Fig. 6). Fig. 6 predicts that during the light adaptation process, when the pupil closes in, first the higher order modes are affected at wavelengths just below cut-off. The first mode is only affected when the pupil closes to within a few tenths of a micrometer.

Absorbance spectrum of the pupil

The pupil granules of fly photoreceptors have a distinct yellow colour, i.e., they have an absorption spectrum that is low at long wavelengths and high at short wavelengths (Vogt et al. 1982). This selective absorption appears to have severe effects on the sensitivity spectrum of a photoreceptor when its pupil is closed. Hardie (1979) measured the spectral sensitivity of blowfly (*Calliphora*) R1–6 photoreceptors in both the dark- and orange-light-adapted state and found that the dark-adapted spectrum peaked in the blue-green, whilst the peak of the light-adapted spectrum was shifted towards the blue. The blue shift occurred with a time constant of ca. 2 s, very much like the time constant of optical changes caused by the pupil. A similar shift occurs in the sensitivity spectrum of housefly (*Musca*) photoreceptors (Vogt et al. 1982). Sensitivity spectra measured at different light intensities revealed a consistent peak shift over a three log unit intensity range, very similar to the adaptation range of the intracellular pupil measured with optical methods (Roebroek and Stavenga 1990a). The measured spectral changes were attributed to the pupil acting as a spectral light filter, but this hypothesis encountered a serious difficulty, because the difference spectrum between the dark- and light-adapted sensitivity spectra (LRP in Fig. 7) strongly deviated from the absorbance spectrum of the pigment in the granules obtained by microspectrophotometry (MSP in Fig. 7). To resolve the enigma, Vogt et al. (1982) argued that the pupil could only filter the light flux propagating outside the rhabdomere. Indeed, multiplying the absorbance spectrum measured optically with a factor $\zeta_1(\lambda) = 1-\eta_1(\lambda)$, i.e. the fraction of the light power of mode 1

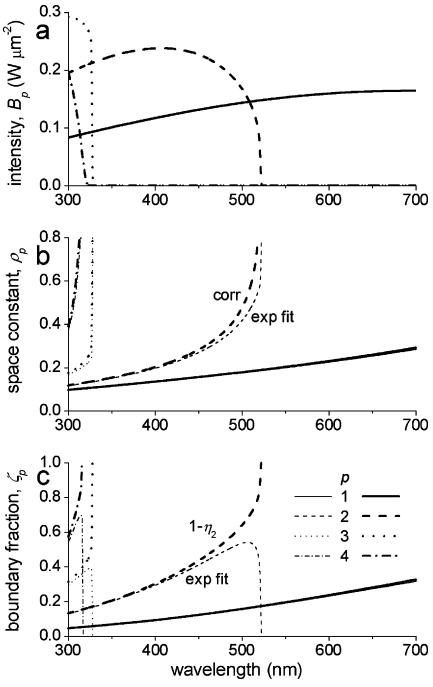

Fig. 5a–c Intensity and spatial distribution of the boundary waves of the different modes, $p = 1$–4, as a function of wavelength. **a** Intensity at the border of the 1.6 µm rhabdomere, B_p. **b** Space constant, ρ_p, obtained by fitting an exponential function to the boundary wave (exp fit; Eq. A7) and corrected space constant (corr; Eq. A9). **c** Total power in the boundary wave following from the exponential fit (exp fit; Eq. A8) and exact value (Eq. A6b). Near the cut-off wavelengths, which for modes $p = 2$, 3 and 4 are 521, 327 and 326 nm, respectively, deviations occur, which inspired the correction of the space constant in b. Each mode propagates a total of 1 W light power at all wavelengths

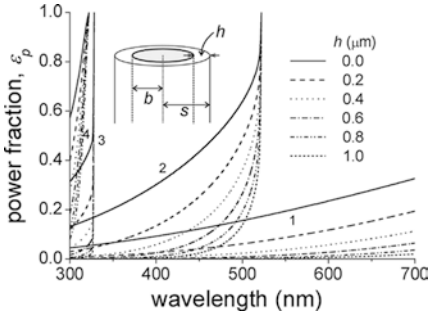

Fig. 6 Wavelength dependence of the light power of different modes outside the rhabdomere. Fraction of the light power in the boundary wave outside a circle cylinder with radius $s = b + h$, calculated with Eq. A15, where the rhabdomere radius $b = 0.8$ µm, and h is the distance between that circle cylinder and the rhabdomere (see inset). In the visible wavelength range less than 10% of the total light power in the first mode propagates outside a cylinder with radius $b + 0.2$ µm ($= 1$ µm). In the higher order modes much larger fractions of the light power propagate outside the rhabdomere, especially near the cut-off wavelengths

propagating outside the rhabdomere, yielded a spectrum resembling the absorbance difference spectrum deduced from the electrophysiological experiments. This approach needs a reassessment, because the single mode case only applies for axial illumination, and when higher

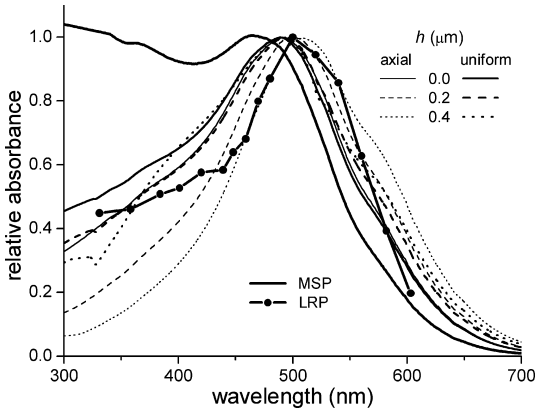

Fig. 7 Normalized absorbance spectra of the fly pupil. The spectrum determined by microspectrophotometry (*MSP*) strongly deviates from that derived from spectral sensitivity measurements of the receptor potential (*LRP*) in both the dark- and light-adapted state (from Vogt et al. 1982). The normalized absorbance spectra that follow from modelling for pupils with distances $h = 0.0$, 0.2 and 0.4 µm are given for both the case of axial illumination and uniform illumination (from Fig. 8)

order modes exist, they will be absorbed rather than the first mode.

Following Roebroek and Stavenga (1990b), who concluded from experimental evidence that the pupil is effectively concentrated distally in the fly photoreceptors, the pupil is treated as a light-absorbing filter placed in front of the rhabdomere. The action of the filter depends on the propagated mode and on three additional factors: the distance of the pupil to the rhabdomere border, h, the absorption spectrum of the granules' pigment, $\alpha_s(\lambda)$, given by the MSP spectrum of Fig. 7, and its concentration, given by a model factor m_s (Eq. A20).

Let us first consider the case of an axial point source, when (virtually) only one mode propagates. The uppermost curve of Fig. 8a repeats the effective light power for the pupil-less case of Fig. 3 (indicated there by P_{eff}, taper). Pupil closure reduces the transmittance of the pupil for mode 1, T_1 (Eq. A16), and thus the effective power (Fig. 8a, calculated with Eqs. A18–A20). The effective power progressively drops except in the red, because the pupil absorbs relatively little at the longer wavelengths. Division of the effective power for the different pupil states (Fig. 8a) by the effective power for the pupil-less case ($h = \infty$), and then taking the negative decadic logarithm of the ratio (Eq. A22) yields the absorbance spectrum of the pupil (Fig. 8b). The parameter that determines the density of the pigment granules ($m_s = 50$, Eq. A20) was chosen so that the pupil absorbance for $h = 0$ reaches a peak value of about 3, in accordance with Roebroek and Stavenga (1990a).

With a uniform light source, the second mode contributes quite appreciably (Fig. 4). The curves of Fig. 8c represent the effective light power spectra in the various states of the closing pupil. The uppermost curve of Fig. 8c ($h = \infty$) gives the effective light power in the

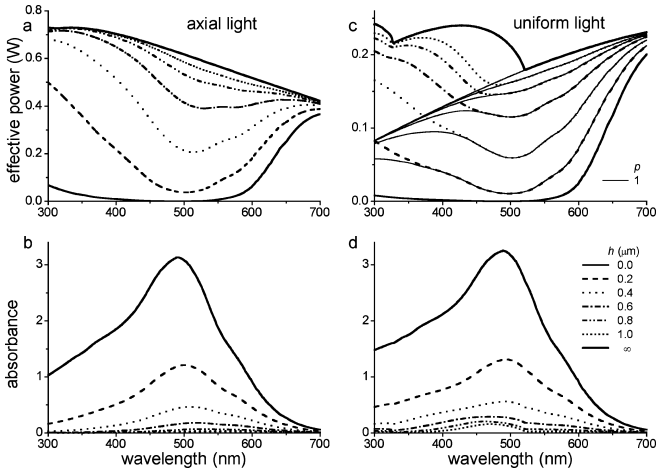

Fig. 8 Effective light power and pupil absorbance spectra for axial (**a**, **b**) and uniform (**c**, **d**) illumination in the tapering rhabdomere of Fig. 3 at various states of pupil closure, given by the value of the pupil distance h. **a** Effective light power spectra with an axial point source delivering 1 W power through the facet lens at all wavelengths. **b** The pupil absorbance spectra resulting from the spectra in a by taking the negative decadic logarithm of each spectrum with respect to the effective power spectrum when the pupil is absent ($h = \infty$; *uppermost curve* in **a**). **c** Effective light power spectra with a uniform light source delivering 1 W sr^{-1} μm^{-2} at the facet lens at all wavelengths. The *bold* spectra are the sum of all mode components. The contribution of mode $p = 1$ is presented by the *thin lines*. **d** The pupil absorbance spectra calculated from the sum spectra in **c** by taking the negative decadic logarithm of each effective power spectrum with respect to the effective power spectrum when the pupil is absent ($h = \infty$; *uppermost curve* in **c**). With axial illumination the pupil interacts at virtually all wavelengths only with one mode, the power of which gradually diminishes with progressive closure of the pupil. With uniform light, the second mode is present to a considerable extent at the shorter wavelengths, so that the closing pupil first reduces the power in that mode, and later it absorbs more from the first mode. The concentration of pupillary pigment has been chosen so that at extreme pupil closure the pupil peak absorbance is ca. 3

1.6 μm rhabdomere with a negligible pupil (identical to Fig. 4c, sum). The thin, continuous lines represent the effective light power spectrum propagating in the lowest order mode ($p = 1$). The latter spectra coincide with the total effective power spectra above 521 nm, the cut-off wavelength of mode $p = 2$. The total effective power spectra again yield the absorbance spectra for the different pupil states, with Eq. A22 (Fig. 8d).

Although the effective light power spectra for the axial and uniform light sources (Fig. 8a and c) look quite different, the resulting pupil absorbance spectra are rather similar (Fig. 8b and d), having all a distinct peak in the blue-green. However, they deviate appreciably from the absorbance spectrum of the pigment in the pupil granules, which is more or less flat in the short wavelength range (MSP, Fig. 7). As expected, the pupil absorbance rises sharply when h, the pupil distance, drops below 0.5 μm. The absorbance spectra for the three pupil states with $h < 0.5$ μm are drawn normalized in Fig. 7, for both cases of illumination. Although the normalized spectra somewhat vary, they resemble the pupil absorbance spectrum derived electrophysiologically (Fig. 7, LRP). Given the experimental errors inherent to the latter spectrum and considering the strongly simplified model for the pupil, the correspondence between the spectra in Fig. 7 underscores the conclusions of Hardie (1979) and Vogt et al. (1982) that closure of the pupil causes changes in the photoreceptor sensitivity spectra as described in detail in the next section.

Spectral sensitivity changes caused by a closing pupil

The absorption spectrum of blowfly visual pigment consists of two components, a band with a peak at 490 nm due to the rhodopsin proper and a band with a peak in the UV due to the sensitizing or antenna pigment. The rhodopsin spectrum of Fig. 9a was calculated by using a visual pigment template (Stavenga et al. 2000), and the sensitizing pigment spectrum was derived from measurements of Hamdorf et al. (1992). The amplitude of the UV-band in Fig. 9a has been chosen about equal to that of the rhodopsin band to approximate the spectral data of Vogt et al. (1982). The peak absorption coefficient of the rhodopsin can be taken to be $\kappa_{v,max} = 0.005$–0.006 μm^{-1} (Warrant and Nilsson 1998), and the length of the rhabdomeres of the blowfly *Calliphora* is about $L = 250$–300 μm (Hardie 1985). Implementation of $\kappa_{v,max}L = 1.5$ in Eq. A18 for the integrated optical system of the 31 μm facet lens - 1.6 μm rhabdomere, together with the excited mode power $P_{p,exc}$, effective mode fraction $\bar{\eta}_p$, and pupil transmittance T_p of the various modes of Fig. 8a and c, yields the total absorbed power P_{abs} for axial (Fig. 9b) and uniform illumination (Fig. 9c).

A comparison of the dark-adapted absorption spectra (Fig. 9b, c; $h = \infty$) and the visual pigment spectrum (Fig. 9a) shows that the overall shape of the absorption spectrum is maintained, but the trough near 400 nm is less deep. This effect, known as self-absorption or self-screening, is due to the exponential (Lambert-Beer) factor of Eq. A17. With a uniform light source, the second mode substantially contributes to the total light flux at short wavelengths. Its effective mode fraction, $\bar{\eta}_1$, is smaller than $\bar{\eta}_2$, and this causes the slightly lower UV peak relative to the peak in the blue-green in Fig. 9c. Note that the absorbed power spectrum features a notch at 521 nm, the cut-off wavelength of the second mode (Fig. 9c).

The pupil acts as a spectral filter. With axial illumination, it causes a gradual blue shift of the absorption peak in the blue-green (Fig. 9b). This contrasts with uniform illumination, where a moderately activated pupil ($h = 1.0$ μm) substantially reduces the absorption in the blue-green, because it extinguishes the second mode there, whilst it has virtually no effect yet in the UV. A more strongly activated pupil ($h < 0.6$ μm) also affects the first mode. For both axial and uniform light, the pupil reduces the absorbed power much more severely in the blue-green than in the ultraviolet.

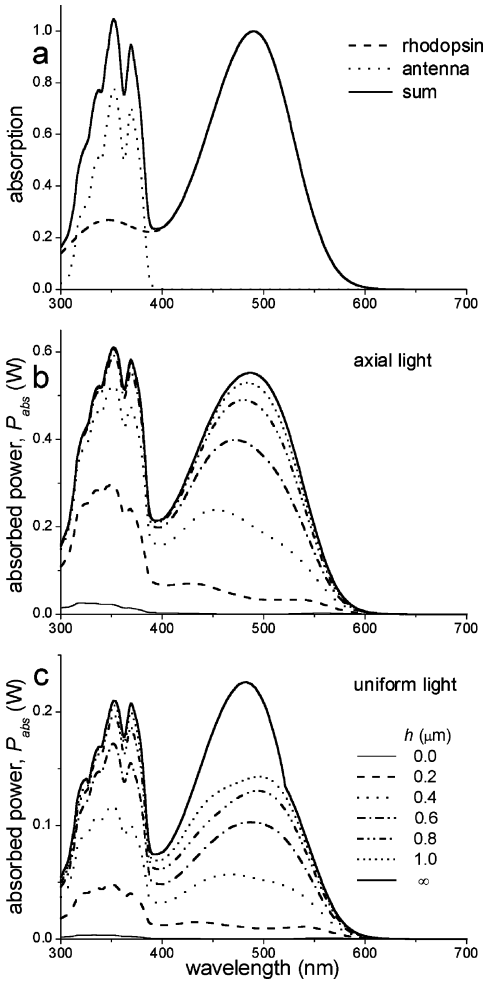

Fig. 9a–c The effects of pupil closure on the spectral sensitivity of fly R1–6 photoreceptors. **a** Fly R1–6 visual pigment consists of a rhodopsin, with peak absorption at 490 nm and a minor side band in the UV, and a sensitizing or antenna pigment, absorbing exclusively in the UV. **b** The power absorbed by the visual pigment with total peak absorption coefficient $\kappa_{v,max}L = 1.5$ concentrated in the tapering rhabdomere of Fig. 3, filtered by the pupil at different states of pupil closure, with 1 W of axial light passing the facet lens at all wavelengths. **c** The same as **b** but with a uniform light source delivering 1 W sr^{-1} μm^{-2} at all wavelengths. Pupil closure progressively depresses the light power absorbed by the visual pigment in the blue-green band, whereas the absorption in the UV is left relatively unaffected

Angular sensitivity changes caused by a closing pupil

Figure 10 shows the angular dependence of the absorbed light power calculated for a monochromatic point source, with wavelength 355 nm and 1 W power focused by the 31 μm facet lens on the 1.6 μm rhabdomere, which contains the same visual pigment density as in Fig. 9. With a focal distance $f = FD_l = 77.5$ μm, the angle spanned by the rhabdomere radius is then $\theta_0 = \arctan(b/f) = 0.59^o$ (indicated by vertical lines in Fig. 10a–c).

Figures 10a and b give the angular dependence of the absorbed power for both allowed modes ($p = 1$ and $p = 2$, respectively), for the different degrees of pupil closure,

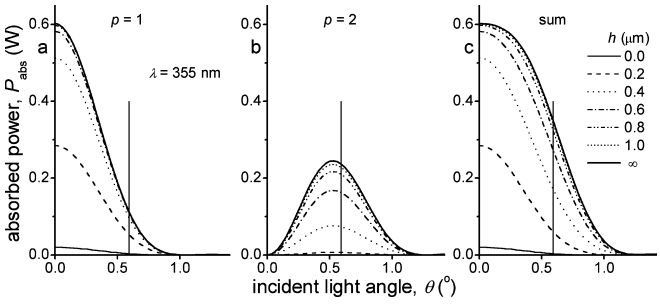

Fig. 10 Light power absorbed at 355 nm, by the visual pigment of Fig. 9 contained in the tapering rhabdomere of Fig. 3, as a function of illumination angle for the first mode (**a**), the second mode (**b**), and their sum (**c**), for the various states of pupil closure. The *thin vertical lines* indicate the angle of the rhabdomere border, $\theta_0 = \arctan(b/f) = 0.59^o$, where the rhabdomere radius is $b = 0.8$ μm, and the focal distance is $f = 77.5$ μm. 1 W of light power emitted by a point source passes the facet lens for each value of the angle θ of the incident light beam

and Fig. 10c presents the angular dependence of the total absorbed power. Pupil closure diminishes mode 2 much more than mode 1, because of the dramatically different angular dependencies of the two modes (Fig. 10a, b). When h drops from 1.0 to 0.4 μm, the total absorbed light power only slightly decreases in peak amplitude, but its angular width noticeably narrows (Fig. 10c).

Normalization of the total absorbed power as a function of angle yields the angular sensitivity functions. Figure 11 presents the angular sensitivities calculated for 355, 494 and 588 nm light together with experimental data of Smakman et al. (1984; their Fig. 5). The experimental and calculated angular sensitivities for 355 nm in the dark-adapted (DA) state closely agree, except at the larger angles (Fig. 11a); the measured angular sensitivity data in the light-adapted (LA) state is well described by a curve calculated for $h = 0.5$ μm (Fig. 11d). With 494 nm light, the experimental data for the dark-adapted state coincide with the calculated curve, but the experimental data for the light-adapted state slightly deviate from the curves calculated for $h = 0.0$ to 1.0, which are virtually identical (Fig. 11b, e). For 588 nm light the experimental data for both dark and light adaptation fully conform to the calculated angular sensitivity curves, which are of course identical because only one mode is allowed at 588 nm (Fig. 11c, f).

A photoreceptor's angular sensitivity is usually characterized by the acceptance angle, the halfwidth of the Gaussian fit, $\Delta\rho$. Figure 12 presents $\Delta\rho$-values produced by fitting Gaussian functions to the angular sensitivity functions calculated for different wavelengths, from 300 to 700 nm, for the same facet lens and rhabdomere system as before, and for different states of pupil closure, expressed by h. The bold curves are obtained using the visual pigment density of the previous section ($\kappa_{v,max}L = 1.5$). The thinner curves assume a sufficiently low visual pigment density so that a linear approximation of the Lambert-Beer exponential function is allowed (Eq. A18). When visual pigment density is high (Fig. 12,

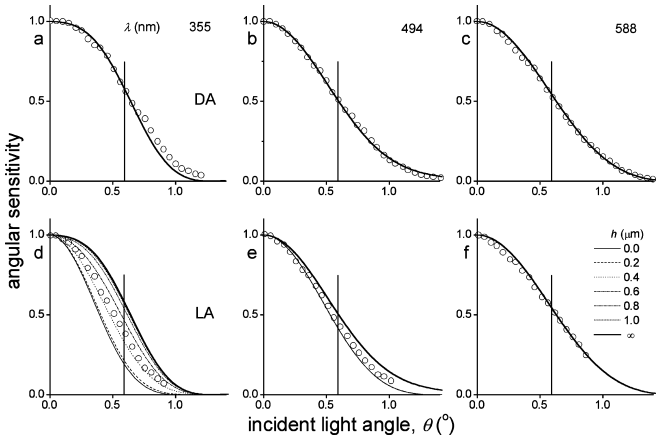

Fig. 11 Angular sensitivity at wavelengths 355 (**a**, **d**), 494 (**b**, **e**) and 588 nm (**c**, **f**) in the dark-adapted (**DA**; **a**, **b**, **c**) and light-adapted state (**LA**; **d**, **e**, **f**), compared to electrophysiological measurements (cell C of Smakman et al. 1984; *open symbols*). The *bold curves* ($h = \infty$) refer to the dark-adapted case, where the pupil is negligible. Light-adaptation causes pupil closure, resulting in narrowing of the angular sensitivity curve, except at 588 nm where only one mode is allowed. The curves of **d** are the normalized curves of Fig. 10c. The *thin vertical lines* indicate the angle of the rhabdomere border

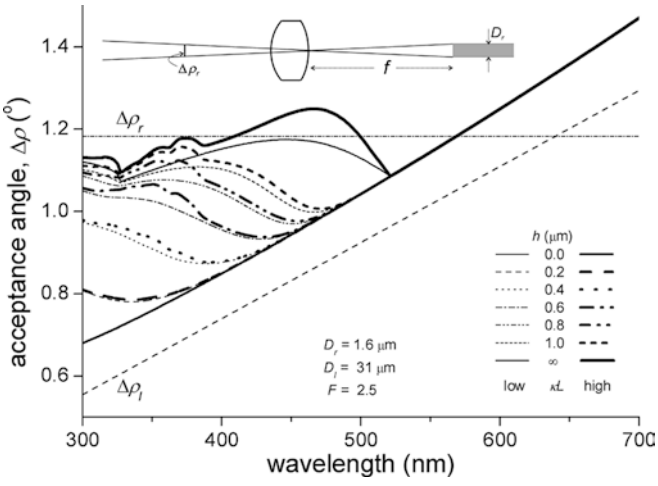

Fig. 12 Angular sensitivity, expressed as the acceptance angle $\Delta\rho$, as a function of wavelength for the different states of the pupil in two cases of visual pigment concentration (low and high). The *bold curves* are the $\Delta\rho$'s of Gaussian fits to curves of the absorbed light power as those in Fig. 10c, where visual pigment absorption is high (κL high). The *thin lines* are $\Delta\rho$'s of fits to the effective light power as a function of illumination angle. The latter yields the same values as obtained by fitting the absorbed power as a function of illumination angle when visual pigment absorption is low (κL low). The *horizontal dash-dot line* represents the geometrical acceptance angle of the rhabdomere $\Delta\rho_r = D_r/f = 1.18^\circ$, where D_r is the rhabdomere diameter and f the focal distance of the facet lens (*inset*). $\Delta\rho_r$ is approximately identical to the angular sensitivity in the dark-adapted state, when the pupil is negligible ($h = \infty$). Upon pupil closure, the angular sensitivity diminishes in the short wavelength range, ultimately approximating the limit set by the first mode and lens diffraction. $\Delta\rho_l = \lambda/D_l$ is (approximately) the angular halfwidth of the Gaussian fit to the lens diffraction pattern

κL high), $\Delta\rho$ is a few percent higher than when density is low (κL low) at short wavelengths, because of self-absorption, and this difference decreases when the pupil closes. The horizontal line in Fig. 12 represents $\Delta\rho_r = 2\theta_0 = 1.18^\circ$, i.e., the angle spanned by the rhabdomere diameter (see Fig. 12, inset). In the fully dark-adapted state, $\Delta\rho$ meanders around the value of $\Delta\rho_r$ in the spectral range of the visual pigment, 300–600 nm (Fig. 12, $h = \infty$). In the fully light-adapted state, $\Delta\rho$ increases monotonically with wavelength (Fig. 12, $h = 0$). The pupil has then completely extinguished the second and higher order modes, so that the angular sensitivity is determined by the diffraction at the facet lens aperture and the first mode. A Gaussian fit to the lens' Airy diffraction pattern yields an angular halfwidth $\Delta\rho_A = 0.99\lambda/D_l$, although it is convenient to use the customary approximation $\Delta\rho_l = \lambda/D_l$ (see Fig. 12). The angular sensitivity of the investigated photoreceptor with the 1.6 μm rhabdomere having a single mode appears to be well approximated by $\Delta\rho = 1.14\Delta\rho_l$. This fully confirms van Hateren (1984), who concluded from his theoretical work and optical measurements that the angular sensitivity of a 1.8 μm rhabdomere carrying one mode at 550 nm is close to the diffraction limit, yielding $\Delta\rho = 1.18\Delta\rho_l$.

Discussion

Pupil absorbance spectrum and photoreceptor spectral sensitivity

Vogt et al. (1982) measured the absorbance spectrum of the pigment in the pupil granules by microspectrophotometry, and found it to be considerably different from a spectrum deduced from electrophysiological measurements. They explained the difference between the two spectra as a waveguide effect by assuming that the progressive decrease of the light power fraction in the boundary wave with decreasing wavelength reduces the action of the pupil at short wavelengths. Vogt et al. (1982) took only the first mode into account and assumed that the power in the boundary wave interacting with the pupil is proportional to $1\text{-}\eta_1 = \zeta_1$. This assumption only holds for a fully closed pupil, however. Furthermore, in the electrophysiological experiments an extended, although possibly not uniform light source was used, which will have channeled a substantial amount of light in the second waveguide mode in the short to middle wavelength range (Fig. 8). Nevertheless, the more complete analysis of the present paper, which included partially closed pupils as well as the higher order modes, fully endorses the conclusion that the light-adapting pupil strongly modifies the photoreceptor sensitivity spectrum.

The calculated pupil absorbance spectra (Fig. 8b, d) strikingly resemble the absorbance spectra derived from antidromic transmission measurements in various states of pupil closure by Roebroek and Stavenga (1990a; their Fig. 3). The absorbance spectra measured in different states of adaptation were found not to be proportional, which was hypothesized to be due to differential absorption of waveguide modes, a theme amply treated

above. Unfortunately, the data of Roebroek and Stavenga (1990a) cannot be properly modeled, because it is obscure to what extent the more or less diffuse antidromic illumination excites the different waveguide modes.

Roebroek and Stavenga (1990a) simultaneously measured the transmission and reflection from the full set of photoreceptors of several ommatidia in different states of light adaptation. The intensity threshold for transmission changes appeared to depend strongly on the wavelength of the antidromic test light, with a minimum near 500 nm and a maximum around 580 nm (Fig. 4 of Roebroek and Stavenga 1990a). This wavelength dependence is immediately understood by comparing it with the present Fig. 6. At long wavelengths only one mode exists, which extends further outside the rhabdomere with increasing wavelength (Fig. 5b). The second mode, existing exclusively in the shorter wavelength range, has similar wavelength dependence. It also increasingly extends outside the rhabdomere with increasing wavelength, but much further than the first mode, which causes a lowered intensity threshold for the pupil. This predicts that the pupil granules will more readily absorb the boundary wave with increasing wavelength, and that there is an abrupt change in the pupil threshold at the cut-off wavelength of the second mode, similar to the sharp transition in the power fraction outside the rhabdomere in Fig. 6. A sudden change in the spectrum of the intensity threshold was not obtained by Roebroek and Stavenga (1990a), however, because the antidromic transmission measurements integrated over all R1–6 photoreceptors, which have rhabdomeres with a slightly varying diameter, 1.5–1.8 μm, meaning cut-off wavelengths of the second mode varying from 489 to 586 nm. Furthermore, the threshold estimation is affected by the relative power in the first and second mode, and the power in the second mode dwindles at wavelengths approaching cut-off.

Angular sensitivity

The calculations of the angular and spectral sensitivities of a photoreceptor have been performed with values for the facet lens and rhabdomere diameter that were deduced from numerical fits on angular sensitivities measured on a specific blowfly photoreceptor (cell C of Smakman et al. 1984). The fits were based on a wave optics model for a rhabdomere whose tip is placed in the focal plane of the facet lens (van Hateren 1984), whilst in the numerical analysis of the angular sensitivity relative weighting factors of the power absorbed from each mode were determined as free parameters. The present work extends the earlier work by including the spectral filtering by the tapering rhabdomere and the self-absorption of the visual pigment in the long rhabdomere. The extended model produces theoretical angular sensitivities conforming satisfactorily to the measured data.

A few discrepancies remain. For instance, the F-number used here, $F = 2.5$, is above the range $F = 2.0 \pm 0.2$ determined by direct optical measurements on isolated blowfly facet lenses (Stavenga et al. 1990). The discrepancy may be due to the assumption of Smakman et al. (1984) that the rhabdomere tip coincides with the focal plane of the facet lens. Although this will in general be a fair approximation, there is considerable flexibility in the position of the rhabdomere tip, because the excited mode power is very robust to displacement of the rhabdomere from the focal plane (Stavenga 2003a). The formalism developed in the latter paper allows a straightforward calculation of the angular sensitivity for rhabdomeres with tip out of focus. Smaller F-numbers can then yield curves that equally well fit the measured data with fewer deviations in the tail (like in Fig. 11a). Furthermore, Smakman et al. (1984) reported pronounced side bands in the experimentally measured angular sensitivity curves. These may, at least in part, be due to spherical aberration. A perfect, aberrationless facet lens was assumed in the previous as well as present modeling, which may be not fully adequate. Accounting for spherical aberration in the theoretical model, by adding a fourth power space term in the exponent of the electric field integral (Eq. 33 of Stavenga 2003a), produces enhanced side bands in the calculated angular sensitivity curves. One could finally remark that the light-adapted angular sensitivity measured at 494 nm (Fig. 11e) is wider than predicted, possibly indicating that the cut-off wavelength of the second mode is not at 521 nm but at a somewhat longer wavelength. Further experimental data are necessary for a detailed assessment of how the geometric values of the facet lens-rhabdomere system and other optical factors, as e.g. defocus, dispersion and spherical aberration, together determine the angular sensitivity. Such an analysis can be postponed, because the principal aim of the present paper is to gain insight how the pupil mechanism affects the light sensitivity of fly photoreceptors, specifically their angular and spectral sensitivity.

The previous modeling studies concluded that the acceptance angle of dark-adapted fly photoreceptors approximates the geometrical angle of the rhabdomere, or, $\Delta\rho = \Delta\rho_r = D_r/f$ (Stavenga 2003a, 2003b). Not surprisingly this conclusion is reconfirmed here, at least when the distal rhabdomere diameter is sufficiently large so that higher order modes contribute in the wavelength range of the visual pigment. The analysis presented here shows that as the pupil reduces the higher order modes $\Delta\rho$ tends towards the diffraction limit of the facet lens. However, even when the pupil is fully closed some broadening of the diffraction limit $\Delta\rho_l = \lambda/D_l$ occurs, depending on the diameter of the rhabdomere and the facet lens' F-number. For the combination of lens and rhabdomere treated in the present paper $\Delta\rho = 1.14\lambda/D_l$. In the central rhabdomeres, R7, 8, only one mode exists virtually always (Stavenga 2003a, 2003b). Consequently, the pupil does not affect the shape of the angular sensitivity curve.

Modelling the fly pupil mechanism

Although the angular and spectral properties of fly photoreceptors and their dependence on the pupil can now be understood within a general, quantitative framework, some caution is still necessary, because the model is grounded on numerous assumptions. A main questionable assumption concerns the distribution of the pupil granules in the different light adapted states. The model considers the pupil and the rhabdomere as a rotational symmetric system, and this is far from realistic. Each of the R1–6 rhabdomeres is positioned at the corner of a trapezoid and the soma containing the granules occupies at most 60° and often much less of the total 360° cross-section (see Appendix 2). The assumption of a sharp front line behind which the granules are distributed homogeneously will also not represent the real situation. All the same, this approximation is probably quite acceptable, because the tiny granules are much smaller than the light wavelength and, due to some randomness, they will act together as a homogeneous mass. This mass will have a spread-out front line, but, given the steep fall in light intensity outside the rhabdomere, it will seem as if the pupil front is abrupt. Furthermore, the pupil granules are definitely not restricted to a fully distal plane, but they are distributed longitudinally in the photoreceptor soma over a distance of at least 20 μm. The experiments of Roebroek and Stavenga (1990b) nevertheless provided strong evidence that the pupil transmittance is effectively equal to the pupil-induced reduction in light sensitivity of the photoreceptor measured electrophysiologically. The results also suggested that gradients in the phototransduction system, which probably occur along the rhabdomere in the light-adapted state, can be neglected.

Simultaneous effects of the pupil on the angular and spectral sensitivities of fly photoreceptors

The absorbance spectrum of the pigment contained in the pupil granules was obtained by microspectrophotometry on squash preparations (Vogt et al. 1982). Wavelength-dependent scattering may have affected the measurements, and therefore the actual absorbance spectrum of the pupil pigment can slightly differ from that used in the calculations. A small shift in the slope of the MSP spectrum of Fig. 7 in the range 500–600 nm noticeably affects the calculated photoreceptor sensitivity spectra, and therefore the pupil-induced changes in the sensitivity spectra may be somewhat different from those shown in Fig. 9.

Figure 9 predicts slightly different spectra for axial and uniform illuminations, and especially a notch in the sensitivity spectrum at the cut-off wavelength of the second mode. Very accurate, detailed spectral measurements are required to put this prediction to the test, but it should be noted that leaky modes (Snyder 1974), which have not been included in the present analysis, will have a smoothing effect on the absorption spectra.

Upon pupil closure the UV-sensitivity strongly increases relative to the sensitivity at longer wavelengths (Fig. 9), as experimentally demonstrated (Hardie 1979; Vogt et al. 1982). The question still is, do these changes also occur in real life? Järemo Jonson et al. (1998) investigated the pupil mechanism of several fly species and compared each pupil's working range with the intensities occurring in the fly's natural environment. Remarkably, all flies appear to have pupil mechanisms with working ranges extending to intensities well above the upper limit of their habitat. The data of Järemo Jonson et al. (1998) for the blowfly *Calliphora* together with those of Roebroek and Stavenga (1990a) for the intensity dependencies of the receptor potential and the pupil indicate that the highest intensity in the habitat causes a maximum pupil absorbance of ca. 1–1.5 log units, values about that of the pupil spectra of Fig. 8b and d with $h \approx 0.2$ μm. The corresponding photoreceptor sensitivity spectra show a high UV band (Fig. 9b, c), and the acceptance angles are then distinctly reduced at short wavelengths (Fig. 12). This suggests that the photoreceptors of flies in their natural habitat have angular and spectral sensitivities that are distinctly modified with respect to the dark-adapted values.

Acknowledgements This study was financially supported by the EOARD. Drs R.C. Hardie and E. Warrant provided extensive and very helpful criticisms. I especially thank Dr S.B. Laughlin for incisive comments and editorial guidance.

Appendix 1: intensity distribution of waveguide modes

Light propagates in a cylindrical optical waveguide in modes, where the light power exists partly inside and partly outside the cylinder. Each mode has a specific mode propagation constant, β:

$$\beta = n_e k = \sqrt{n_1^2 k^2 - \left(\frac{U}{b}\right)^2} = \sqrt{n_2^2 k^2 + \left(\frac{W}{b}\right)^2} \qquad (A1)$$

where b is the rhabdomere radius; n_e is the effective refractive index of the waveguide for the propagated mode, and n_1 and n_2 are the refractive indices of the media inside and outside the waveguide; k is the wave number, where $k = 2\pi/\lambda$, with λ the light wavelength; U and W are the roots of the characteristic waveguide equation (Snyder 1969):

$$U\frac{J_{l+1}(U)}{J_l(U)} = W\frac{K_{l+1}(W)}{K_l(W)} \qquad (A2)$$

where J_l and K_l are (modified) Bessel functions. U and W together determine the waveguide number V (with Eq. A1):

$$V = \sqrt{U^2 + W^2} = kb\sqrt{(n_1^2 - n_2^2)} = \frac{\pi D_r}{\lambda}\sqrt{(n_1^2 - n_2^2)} \qquad (A3)$$

where $D_r = 2b$ is the diameter of the rhabdomere. The number of allowed modes depends on the cut-off V-number, V_{co}, which is 2.405, 3.832, 3.847 and 5.136 for modes $p = 1$, 2, 3 and 4, respectively (for mode nomenclature and the value of parameter l for mode p, see Table 2 of Stavenga 2003a).

When unpolarized, monochromatic incident light excites a total power of $P_p = 1$ W in mode p, the average intensity of this mode is given by:

$$\bar{I}_p^*(R) = \left|M_p^*(R)\right|^2 H(U,W)/\pi b^2 \qquad (A4a)$$

with

$$M_p^*(R) = J_l(UR)/J_l(U), \quad R \leqslant 1 \qquad (A4b)$$

$$M_p^*(R) = K_l(WR)/K_l(W), \quad R \geqslant 1 \qquad (A4c)$$

and

$$H(U,W) = -\frac{W^2}{V^2}\frac{J_1^2(U)}{J_{l-1}(U)J_{l+1}(U)} \qquad (A4d)$$

where $R = r/b$ is the radial distance from the waveguide axis, r, normalized to its radius value. The mode intensity at the rhabdomere border ($r = b$, or $R = 1$) is:

$$B_p = \bar{I}_p(b) = \bar{I}_p^*(1) = H(U,W)/\pi b^2 \qquad (A5)$$

because $M_p^*(1) = 1$. The physical quantities are adorned with an asterisk when the expressions are given as a function of the normalized spatial coordinate, R. They are without an asterisk when the spatial coordinate is r; e.g., $\bar{I}_p^*(R) \equiv \bar{I}_p(r)$ and $M_p^*(R) \equiv M_p(r)$. Considering Eq. A4a, it may be useful to note that in case the total power of 1 W were confined within the rhabdomere boundary and equally distributed there, the intensity would be $1/\pi b^2$; πb^2 is the cross-sectional area of the rhabdomere.

The fraction of the total light power propagated in mode p inside the rhabdomere follows from spatial integration of Eq. A4 using Eqs. A4b and A4c:

$$\eta_p = (W/V)^2 + H(U,W) \qquad (A6a)$$

and the fraction of the total light power propagated in mode p outside the rhabdomere is:

$$\zeta_p = 1 - \eta_p = (U/V)^2 - H(U,W). \qquad (A6b)$$

The light intensity outside the rhabdomere ($r \geq b$), given by Eq. A4a together with Eqs. A4c and A4d, can be approximated with an exponential function:

$$\bar{\bar{I}}_p(r) = B_p e^{-\frac{r-b}{\rho_p}} \qquad (A7)$$

where r - b is the radial distance to the rhabdomere border and ρ_p is the space constant of mode p. The fraction of the total light power propagated in mode p outside the rhabdomere is then simply derived by spatial integration of Eq. A7, yielding:

$$\zeta_p = 2\pi B_p \rho_p(\rho_p + b). \qquad (A8)$$

The right-hand term of Eq. A8 should formally contain a factor P_p^{-1}, because ζ_p is dimensionless, the dimension of ρ_p and b is μm, and that of B_p is W μm^{-2}, but the factor is omitted here because $P_p = 1$ W. Of course, the shape of the intensity distribution in a mode is independent of the total propagated light power, and when $P_p \neq 1$ W, the intensity B_p is proportionally modified.

Numerical results of Eqs. A6b and A8 are given in Fig. 5c. It appears that the calculation of Eq. A8 with the values of ρ_p derived from the exponential fit, Eq. A7, yields ζ_p values which deviate from the exact values (calculated from Eq. A6b) at wavelengths near cut-off (Fig. 3b). A more correct space constant is obtained by using the exact ζ_p-value and then solving ρ_p from Eq. A8:

$$\rho_p = \left[\sqrt{\frac{b^2}{4} + \frac{\zeta_p}{2\pi B_p}} - \frac{b}{2}\right]. \qquad (A9)$$

ρ_p values calculated with this relation are presented in Fig. 3b (bold curves).

Appendix 2: light absorption by visual pigment and pupil

On its way along a fly rhabdomere, some of the light power is absorbed by the visual pigment inside the rhabdomere and/or by the screening pigment of the pigment granules in the soma, depending on the light wavelength. When the extinction is sufficiently small, so that the intensity distribution in the modes is not strongly affected, Lambert-Beer's law can be applied. If the medium of the rhabdomere interior with the visual pigment is homogeneous and has an absorption coefficient κ_v, and the exterior medium with the screening pigment is equally homogeneous with absorption coefficient κ_s, it is straightforward to prove that the effective absorption coefficient of the rhabdomere is given by (see Snyder 1975):

$$\kappa_p = \kappa_{p,v} + \kappa_{p,s} \qquad (A10a)$$

where

$$\kappa_{p,v} = \eta_p \kappa_v \qquad (A10b)$$

is the effective absorption coefficient for mode p due to the visual pigment, and

$$\kappa_{p,s} = \zeta_p \kappa_s \qquad (A10c)$$

is the effective absorption coefficient due to the pupillary screening pigment.

The assumption of a homogeneous distribution of the screening pigment granules, underlying Eq. A10c, will in general not hold for the photoreceptor soma. When the density of the granules is non-homogeneous and a light

power $P_p = P_p(z)$ flows in mode p through a plane perpendicular to the rhabdomere axis with longitudinal coordinate z, then P_p changes in a layer dz due to absorption by the pupil (with $\bar{I}_p(r) \equiv \bar{I}_p^*(R)$):

$$dP_p = -dz \int_b^\infty \int_0^{2\pi} \kappa_s(r)\bar{I}_p(r) r dr d\varphi = -dz 2\pi \int_b^\infty \kappa_s(r)\bar{I}_p(r) r dr. \quad (A11)$$

Here the pupil is taken to be circular symmetric around the rhabdomere waveguide. This may be well-approximated by the fused rhabdoms of bees and butterflies, but it is less realistic for fly eyes. When the cross-section of the soma of the fly photoreceptor under consideration spans an angle $\Delta\phi_c$, i.e. occupies a fraction $\psi = \Delta\phi_c/2\pi$ of the total 2π, the right-hand term of Eq. A11 has to be corrected by a factor ψ.

Illumination of a dark-adapted fly eye triggers the migration of pigment granules in the photoreceptor from a remote area towards the rhabdomere. A useful case to consider then is that where the pupillary granules are uniformly dispersed outside a cylinder with radius $s = b + h$, so that an annulus with width h is left empty (Fig. 4, inset). Then $\kappa_s(r) = \kappa_s$ for $r >$ s, and $\kappa_s(r) = 0$ for $r < s$, so that Eq. A11 yields:

$$dP_p = -\kappa_s \varepsilon_p(s) P_p dz \quad (A12)$$

where

$$\varepsilon_p(s) = \frac{2\pi}{P_p} \int_s^\infty \bar{I}_p(r) r dr. \quad (A13)$$

Here $\varepsilon_p(s) = \varepsilon_p^*(S)$, with $S = s/b$, can be derived from waveguide theory via spatial integration, with Eqs. A4a, A4c and A4d, yielding:

$$\varepsilon_p^*(S) = S^2 \frac{K_{l-1}(WS)K_{l+1}(WS) - K_l^2(WS)}{K_l^2(W)} H(U, W). \quad (A14)$$

A more accessible expression is obtained with the exponential approximation of the distribution of light intensity outside the rhabdomere, Eq. A7, yielding

$$\varepsilon_p(s) = 2\pi B_p \rho_p (\rho_p + s) e^{-\frac{h}{\rho_p}}. \quad (A15)$$

The much friendlier Eq. A15 is the preferred choice for gaining insight into the interaction of the pupil and the rhabdomere boundary wave, since calculations show that the values obtained from Eqs. A14 and A15 closely correspond for all modes p when using the corrected ρ_p values (Eq. A9, Fig. 3b); only slight deviations occur near the cut-off wavelengths for $h \approx 1$ μm. Fig. 4 presents Eq. A15 for the case of $D_r = 1.6$ μm. When the pigment granules are homogeneously dispersed throughout the soma up to the rhabdomere, so that $s = b$ or $h = 0$, Eq. A15 becomes equivalent to Eq. A8, because $\epsilon_p(b) = \zeta_p$, where ζ_p, the fraction of the mode light power propagated outside the rhabdomere, is given by Eq. A6b.

Appendix 3: light sensitivity

The light sensitivity of a photoreceptor is defined as the fraction of the incident light power absorbed by the visual pigment. A general, simple and/or analytic expression for the light power absorbed by the visual pigment cannot be given, because the granules are distributed over a limited longitudinal distance in the photoreceptor soma, and this distribution will be quite inhomogeneous. Electrophysiological experiments indicate however that the pupil is effectively concentrated distally in the fly photoreceptors (Roebroek and Stavenga 1990b), with the result that the fly pupil is in fact comparable to the case of the pupil in the human eye. The pupil action then may be approximated by that of a set of transmission filters T_p, for each mode p, given by:

$$T_p = e^{-\kappa_{p,s}\delta_s} = e^{-K_{p,s}} \quad (A16)$$

with δ_s the longitudinal distance over which the pupil extends, and where the absorption coefficient $\kappa_{p,s}$ increases with light adaptation proportional to the increase in the number of pigment granules in the boundary wave area.

Let us first consider the case of a fly eye illuminated with a monochromatic point source delivering a total power $P(\lambda) = 1$ W at wavelength λ through a facet lens. The light flux excites a power $P_{p,exc}$ in mode p in the rhabdomere, which is a function of the angle of incidence and wavelength and is calculated by a convolution of the facet lens diffraction pattern and the rhabdomere waveguide modes (Pask and Barrell 1980a, 1980b; van Hateren 1989; Stavenga 2003a, 2003b).

The excited light power is first filtered by the pupil mechanism and then propagates in the rhabdomere until it is eventually absorbed by the visual pigment. The total power absorbed, summed over all modes, is:

$$P_{abs}(\lambda) = \sum_p P_{p,abs}(\lambda) = \sum_p P_{p,exc}(\lambda) T_p(\lambda) \left\{1 - e^{-\bar{\eta}_p(\lambda)\kappa_v(\lambda)L}\right\} \quad (A17)$$

thus yielding the light sensitivity of the photoreceptor; $\bar{\eta}_p$ is the averaged light fraction of mode p propagating inside the rhabdomere (Stavenga 2003b). The angular and spectral sensitivity of the photoreceptor are derived by normalization to the angular or spectral peak values, respectively.

Concerning the angular sensitivity, in Eq. A17 only $P_{p,exc}$ depends on the incident angle of the light source.

When no more than one mode contributes to the light sensitivity, the angular sensitivity at a certain wavelength is independent of the degree of light absorption by the pupillary and visual pigments, due to normalization. This does not hold however when two or more modes are present.

Equation A17 is considerably simplified when $\kappa_v(\lambda)L$ is sufficiently small. Then (Eq. 44 of Stavenga 2003a):

$$P_{abs}(\lambda) = \kappa_v(\lambda)L\sum_p P_{p,eff}(\lambda) = \kappa_v(\lambda)LP_{eff}(\lambda) \qquad (A18)$$

where $P_{p,eff}$ is the effective mode power from which light can be absorbed by the visual pigment (Eq. 45 of Stavenga 2003b):

$$P_{p,eff}(\lambda) = P_{p,exc}(\lambda)T_p(\lambda)\bar{\eta}_p(\lambda). \qquad (A19)$$

In this case the angular sensitivity at a given wavelength is independent of visual pigment absorption and can be obtained directly from P_{eff}, again due to normalization. Figure 10 presents the effective light power for both modes present at 355 nm in the 1.6 μm rhabdomere, as well as their sum.

When the pupil absorption is negligible, $T_p = 1$ for all modes p. This case is illustrated for an axial point source in Fig. 3 and for a uniform light source in Fig. 4. When the illumination comes from a uniform light source, $P_{p,exc}$ in Eq. A17 and A19 is obtained by integrating the excited mode power over the angle of incidence (Eq. A14 of Stavenga 2003b).

Figure 8 shows the spectral changes in effective power due to pupil closure for 6 degrees of pupil closure, indicated by the pupil distance $h = s - b$, and where the exponent of the transmittance (Eq. A16) for mode p is:

$$K_{p,s}(\lambda, h) = m_s\alpha_s(\lambda)\varepsilon_p(\lambda, h) \qquad (A20)$$

where m_s is a factor proportional to the concentration of the pigment, $\alpha_s(\lambda)$ is the normalized absorption coefficient of the pupillary screening pigment (given in Fig. 7), and $\epsilon_p(\lambda,s)$ is the mode power fraction outside the cylinder with radius s (Eq. A15). In the calculations for Fig. 8 a value $m_s = 50$ was chosen so that the maximally closed pupil yielded a peak absorbance of ca. 3 log units (Roebroek and Stavenga 1990a). If the action of the pupil is approximated by that of a filter controlling the light flux distally of the visual pigment, the pupil transmittance is:

$$T(\lambda, h) = \frac{P_{abs}(\lambda, h)}{P_{abs}(\lambda, \infty)} \qquad (A21)$$

where $P_{abs}(\lambda,h)$ is given by Eq. A17, with $T_p(\lambda) = T_p(\lambda,h)$, and $h = \infty$ represents the case where the pupil is negligible. The absorbance of the pupil then follows from:

$$A(\lambda, h) = -^{10}\log T(\lambda, h). \qquad (A22)$$

References

Boschek B (1971) On the fine structure of the peripheral retina and lamina ganglionaris of the fly, *Musca domestica*. Z Zellforsch 118:369–409

Franceschini N (1975) Sampling of the visual environment by the compound eye of the fly: fundamentals and applications. In: Snyder AW, Menzel R (eds) Photoreceptor optics. Springer, Berlin, Heidelberg, New York, pp 98–125

Franceschini N, Kirschfeld K (1976) Le contrôle automatique du flux lumineux dans l'oeil composé des Diptéres. Propriétés spectrales, statiques et dynamiques du mécanisme. Biol Cybern 21:181–203

Hamdorf K, Hochstrate P, Höglund G, Moser M, Sperber S, Schlecht P (1992) Ultra-violet sensitizing pigment in blowfly photoreceptors R1–6; probable nature and binding sites. J Comp Physiol A 171:601–615

Hardie RC (1979) Electrophysiological analysis of the fly retina. I. Comparative properties of R1–6 and R7 and R8. J Comp Physiol A 129:19–33

Hardie RC (1985) Functional organization of the fly retina. In: Ottoson D (ed) Progress in sensory physiology, vol 5. Springer, Berlin Heidelberg New York, pp 1–79

Hateren JH van (1984) Waveguide theory applied to optically measured angular sensitivities of fly photoreceptors. J Comp Physiol A 154:761–771

Hateren JH van (1989) Photoreceptor optics, theory and practice. In: Stavenga DG, Hardie RC (eds) Facets of vision. Springer, Berlin Heidelberg New York, pp 74–89

Hateren JH van, Hardie RC, Laughlin SB, Stavenga DG (1989) The bright zone, a specialized dorsal eye region in the male blowfly *Chrysomia megacephala*. J Comp Physiol A 164:297–30

Järemo Jonson AC, Land MF, Osorio DC, Nilsson D-E (1998) Relationships between pupil working range and habitat luminance in flies and butterflies. J Comp Physiol A 182:1–9

Kirschfeld K (1974) The absolute sensitivity of lens and compound eyes. Z Naturforsch C 29:592–596

Land MF (1989) Variations in the structure and design of compound eyes. In: Stavenga DG, Hardie RC (eds) Facets of vision. Springer, Berlin Heidelberg New York, pp 90–111

Masai I, Suzuki E, Yoon C-S, Kohyama A, Hotta Y (1996) Immunolocalization of *Drosophila* eye-specific diacylglycerol kinase, *rdgA*, which is essential for the maintenance of the photoreceptor. J Neurobiol 32:695–706

Pask C, Barrell KF (1980a) Photoreceptor optics. I. Introduction to formalism and excitation in a lens-photoreceptor system. Biol Cybern 36:1–8

Pask C, Barrell KF (1980b) Photoreceptor optics. II. Application to angular sensitivity and other properties of a lens-photoreceptor system. Biol Cybern 36:9–18

Roebroek JGH, Stavenga DG (1990a) Insect pupil mechanisms. IV. Spectral characteristics and light intensity dependence in the blowfly, *Calliphora erythrocephala*. J Comp Physiol A 166:537–543

Roebroek JGH, Stavenga DG (1990b) On the effective density of the pupil mechanism of fly photoreceptors. Vision Res 30:1235–1242

Smakman JG, Hateren JH van, Stavenga DG (1984) Angular sensitivity of blowfly photoreceptors: intracellular measurements and wave-optical predictions. J Comp Physiol A 155:239–247

Snyder AW (1969) Asymptotic expressions for eigenfunctions and eigenvalues of a dielectric or optical waveguide. IEEE Trans Microwave Theory Tech 17:1130–1138

Snyder AW (1974) Leaky-ray theory of optical waveguides of circular cross section. Appl Phys 4:273–298

Snyder AW (1975) Optical properties of invertebrate photoreceptors. In: Horridge GA (ed) The compound eye and vision of insects. Clarendon Press, Oxford, pp 179–235

Snyder AW (1979) Physics of vision in compound eyes. In: Autrum H (ed) Handbook of sensory physiology, vol VII/6A. Springer, Berlin Heidelberg New York, pp 225–313

Stavenga DG (1979) Pseudopupils of compound eyes. In: Autrum H (ed) Handbook of sensory physiology, vol VII/6A. Springer, Berlin Heidelberg New York, pp 357–439

Stavenga DG (1989) Pigments in compound eyes. In: Stavenga DG, Hardie RC (eds) Facets of vision. Springer, Berlin Heidelberg New York, pp 152–172

Stavenga DG (2003a) Angular and spectral sensitivity of fly photoreceptors. I. Integrated facet lens and rhabdomere optics. J Comp Physiol A 189:1–17

Stavenga DG (2003b) Angular and spectral sensitivity of fly photoreceptors. II. Dependence on facet lens F-number and rhabdomere type in *Drosophila*. J Comp Physiol A 189:189–202

Stavenga DG, Zantema A, Kuiper JW (1973) Rhodopsin processes and the function of the pupil mechanism in flies. In: Langer H (ed) Biochemistry and physiology of visual pigments. Springer, Berlin Heidelberg New York, pp 175–180

Stavenga DG, Kruizinga R, Leertouwer HL (1990) Dioptrics of the facet lenses of male blowflies *Calliphora* and *Chrysomia*. J Comp Physiol A 166:365–371

Stavenga DG, Oberwinkler J, Postma M (2000) Modeling primary visual processes in insect photoreceptors. In: Stavenga DG, DeGrip WJ, Pugh Jr EN (eds) Molecular mechanisms in visual transduction. Handbook of biological physics, vol. 3. Elsevier, Amsterdam, pp 527–574

Trujillo-Cenóz O (1972) The structural organization of the compound eye in insects. In: Fuortes MGF (ed) Handbook of sensory physiology, vol VII/2. Springer, Berlin Heidelberg New York, pp 5–62

Vogt K, Kirschfeld K, Stavenga DG (1982) Spectral effects of the pupil in fly photoreceptors. J Comp Physiol A 146:145–152

Warrant EJ, Nilsson DE (1998) Absorption of white light in photoreceptors. Vision Res 38:195–207

Wunderer H, Smola U (1982) Morphological differentiation of the central visual cells R7/8 in various regions of the blowfly eye. Tissue Cell 14:341–358